Ultraviolet Resonance Raman Spectrometry for Detection and Speciation of Trace Polycyclic Aromatic Hydrocarbons

Sanford A. Asher

Department of Chemistry, University of Pittsburgh, Pittsburgh, Pennsylvania 15260

A novel UV resonance Raman spectrometer has been utilized for the UV resonance Raman study of polycyclic aromatic hydrocarbons (PAH). This work represents the first application of Raman spectrometry to determination of trace polycyclic aromatic hydrocarbons such as napthalene, anthracene, phenanthrene, and pyrene and various substituted derivatives. The data illustrate that UV resonance Raman enhancement is sufficient to study trace levels of these species, down to the 20 ppb level. The factors which determine the detection limit for UV resonance Raman measurements are discussed. The resonance Raman intensities strongly depend upon the excitation wavelength. Thus, by a judicious choice of excitation wavelength it should be possible to selectively excite individual PAH species in mixtures. Resonance Raman studies of anthracene and its 2-methyl, 9-methyl, 9-phenyl, and 9,10-diphenyl derivatives demonstrate that the Raman frequency and intensity differences permit easy differentiation between these structurally similar species. The potential utility of this new technique for the speciation and detection of PAH's in complex matrices is discussed.

Polycyclic aromatic hydrocarbons (PAH) in the environment are a potential health hazard because some of these species are known to induce carcinogenesis (*1*). Significant efforts have been expended to devise techniques for the identification and quantitation of PAH's in complex matrices such as soot, in water, and in soil (*2*). The best techniques at present are mass spectrometry and fluorescence which can detect PAH's at the subpicogram level (*3, 4*). Unfortunately, mass spectrometry, in general, requires significant sample preparation while fluorescence is plagued with matrix effects such as quenching and interference from other luminescent species. Further, the broad fluorescence spectra of PAH's make speciation between very similar chemical species difficult. This can be greatly aided by matrix isolation techniques, but again, significant sample preparation is required.

We have recently embarked on a program to develop UV resonance Raman spectrometry as a new technique for the selective detection and speciation of molecules in complex matrices. In this paper we demonstrate the selectivity and sensitivity of UV resonance Raman spectrometry to low concentrations of a series of PAH's such as napthalene, anthracene derivatives, phenanthrene, and pyrene. Subsequent reports will demonstrate selectivity and sensitivity for PAH's in complex matrices.

The resonance Raman technique has been utilized recently in numerous studies of inorganic complexes (*5, 6*), extensively conjugated macromolecules (*6*), and numerous biomolecules (*7–9*). With the visible-wavelength laser-based Raman instrumentation previously available, the technique was only applicable for chromaphores which absorbed in the visible spectral region. We have surmounted this limitation by constructing a novel UV resonance Raman spectrometer continuously tunable between 217 and 800 nm (*10, 11*). This new instrument permits resonance Raman excitation into the UV absorption bands of PAH's.

Resonance Raman spectrometry differs from normal Raman spectrometry because the laser excitation occurs within an absorption band of the molecule studied. A significant enhancement (often $>10^6$) occurs for the Raman spectrum of the chromaphoric species. Thus, the vibrational spectrum of that one molecular species can be selectively observed. The Raman frequencies are highly sensitive to molecular structure, while the intensities depend upon concentration and upon a variety of detailed molecular parameters such as excited state geometry and vibronic coupling mechanisms present within the ground and excited states (*12–15*). The Raman enhancement mechanism can be identified from the resonance Raman excitation profiles, measurements of the dependence of Raman peak intensities as a function of the excitation wavelength. The excitation profile data can also be used to characterize the selectivity available for resonance Raman studies of an analyte and can be used to select the optimal excitation wavelength for the molecule of interest.

In this study we demonstrate PAH's can be *speciated* at low concentrations, and demonstrate that, given an internal intensity reference, the PAH Raman intensities are linear with concentration over the 4 orders of magnitude measured. The spectra easily differentiate between species as similar as 2-methyl- and 9-methylanthracene which have essentially identical absorption and fluorescence spectra. This work represents a preliminary report; the instrumentation has not been optimized for measurements of low concentrations of PAH's.

EXPERIMENTAL SECTION

PAH samples were a gift from David Hercules and were obtained as standards from Chem Services, West Chester, PA. They were dissolved as stock 10^{-3} M solutions in acetonitrile. Aliquots were drawn to prepare solutions of the required concentrations. The acetonitrile was obtained from Burdick and Jackson. The samples were measured with 90° scattering in a lamellar jet flow stream apparatus which utilized a stainless steel and Teflon micropump and a dye laser jet nozzle measuring 3 mm high and 0.2 mm wide. The sampling jet has been described elsewhere (*11*). The instrumentation used has also been recently described (*11*). It consists of a Quanta Ray 20-Hz DCR2A Nd Yag laser which is frequency doubled or tripled to excite a dye laser (Figure 1). UV excitation is generated either by (1) mixing the dye laser output with the 1064-nm Yag fundamental light, (2) doubling the dye laser light, or (3) mixing the doubled dye laser light with the 1064-nm Yag fundamental. In this way, light between 217 and 450 nm can be generated. Direct output from the dye laser can generate light between 400 and 800 nm. The excitation beam is diffusely focused on the sample by a 10-in. lens in order to avoid nonlinear Raman phenomena. The light is collected with an ellipsoidal mirror and imaged into a modified Spex triplemate monochromator through a crystalline quartz wedge polarization scrambler. The Rayleigh scattered light is rejected in the filter stage of the monochromator using 300 nm blaze, 600 groove/mm gratings in first order; this choice of grating order was required in order to reject PAH fluorescence in the near-UV and visible spectral region. The spectrograph stage used a 1200 groove/mm grating in second order to disperse and image the Raman scattered light onto a PAR Model 1420 intensified Reticon multichannel array. An OMA II console and PAR 1218 controller controlled

0003-2700/84/0356-0720$01.50/0

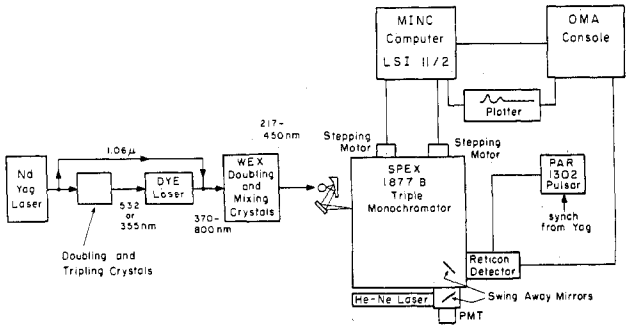

Figure 1. Schematic diagram of the tunable UV resonance Raman spectrometer. See text for details.

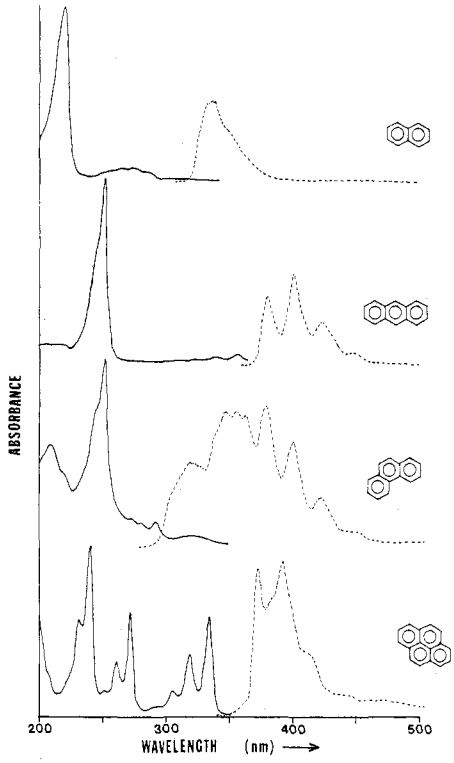

Figure 2. Absorption and fluorescence spectrum of napthalene, phenanthrene, anthracene, and pyrene; fluorescence excitation, 220 nm.

the Reticon array and accumulated the data. A PAR pulser was used to gate the array on during 10-ns intervals which bracketed the laser excitation pulse.

RESULTS AND DISCUSSION

Figure 2 shows the absorption and fluorescence spectra of napthalene, anthracene, phenanthrene, and pyrene dissolved as ca. 10^{-5} M solutions in acetonitrile. As the aromatic ring conjugation increases, the absorption bands as well as the fluorescence bands shift to longer wavelength. In each case fluorescence emission occurs from the lowest singlet excited state and no fluorescence is evident in the 200–300 nm UV spectral region.

Figure 3 shows the resonance Raman spectra of each of these PAH's excited close to the λ_{max} of their strong UV absorption bands. Each of the derivatives shows Raman peaks characteristic of the complex. In the napthalene spectrum the 1377- and 2243-cm^{-1} peaks derive from the solvent CH_3CN. However, these peaks are not evident for the other derivatives because the spectra are dominated by the Raman spectra of the PAH's. Strong peaks at 766, 756, and 745 cm^{-1} are observed for naphthalene, anthracene, and phenanthrene, respectively. Other strong peaks are observed at 399 and 1407 cm^{-1} for anthracene, at 386 and 1386 cm^{-1} for phenanthrene,

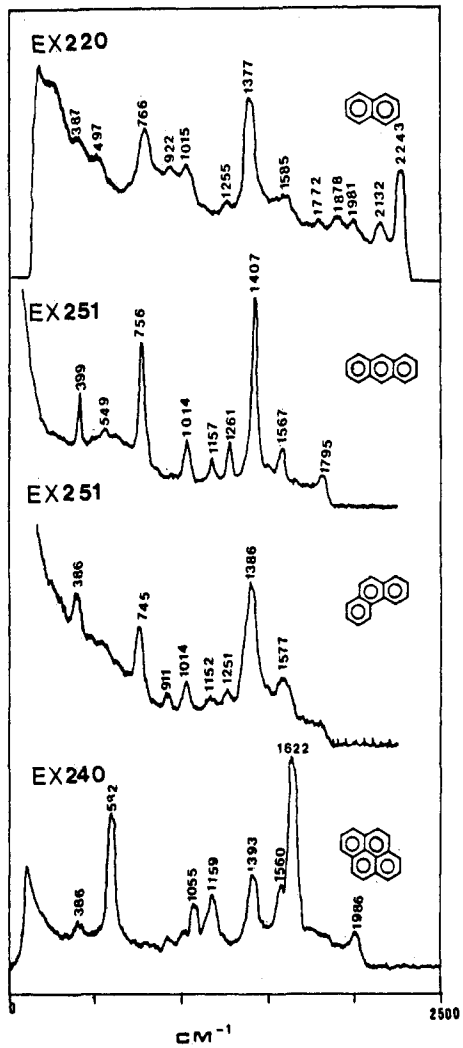

Figure 3. UV resonance Raman spectra of napthalene, anthracene, phenanthrene, and pyrene excited at their absorption band maxima: (napthalene) λ_{ex} 220 nm, average power 12.0 mW, slit width ca. 14 cm^{-1}, number of pulses averaged 12 000, note that this corresponds to a spectrum accumulation time of 10 min: (anthracene) λ_{ex} 251 nm, average power 3.5 mW, slit width $\cong$11 cm^{-1}, number of pulses averaged 12 000; (phenanthrene) λ_{ex} 240 nm, average power 3.0 mW, slit width $\cong$11 cm^{-1}, number of pulses averaged 12 000; (pyrene) conditions identical with those for phenanthrene.

and at 582, 1393, and 1622 cm^{-1} for pyrene. The vibrations most resonance enhanced with UV excitation are also those most important in the electronic transitions giving rise to the absorption spectra. For example, for the ca. 250 nm absorption band of anthracene (see Figure 2) the energy difference between the peak and the short wavelength shoulder is ca. 1400 cm^{-1}; the strongest feature in the anthracene Raman spectra is a peak at 1407 cm^{-1}. In pyrene the shorter wavelength absorption peak occurs at ca. 1600 cm^{-1} higher in energy from the main peak, and a shoulder is observed in the pyrene absorption band at ca. 600 cm^{-1} to higher energy from the main peak; the pyrene Raman spectrum shows two strong peaks at 1622 and 582 cm^{-1}.

Figure 4 shows the concentration dependence of the pyrene resonance Raman spectrum. The upper spectrum is that of CH_3CN, the solvent. The lower four spectra of pyrene were measured at concentrations from 10^{-3} M to 10^{-6} M. As the concentration decreases from 10^{-3} M to 10^{-4} M an increase in intensities of the acetonitrile peaks occur at 380, 918, and 1376 cm^{-1}. All of the spectra shown are plotted on the same intensity scale. Thus, essentially no decrease has occurred in the pyrene Raman intensities between the 10^{-3} and 10^{-4} M solution. The increase in CH_3CN Raman intensity and the

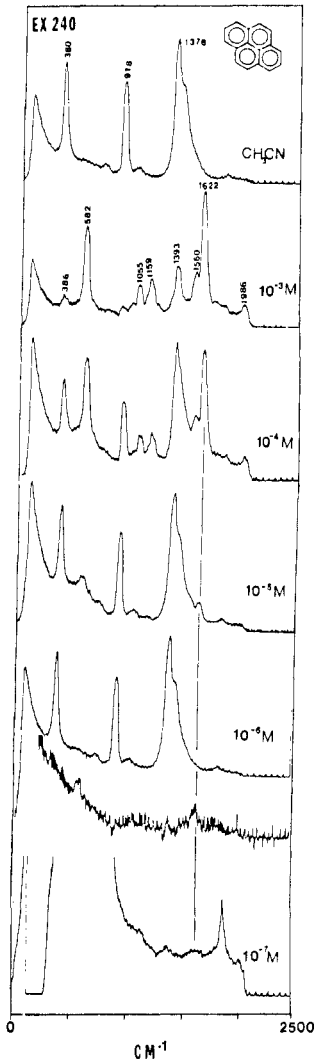

Figure 4. Concentration dependence of UV resonance Raman spectrum of pyrene. Top spectrum is of pure CH_3CN. Experimental conditions are identical for all concentrations measured except for the 10^{-7} M solution of pyrene in H_2O: λ_{ex} 240 nm, average power 3.0 mW, slit width $\cong$11 cm^{-1}, number of pulses averaged 12 000. Experimental conditions for 10^{-7} M aqueous pyrene solution are as follows: λ_{ex} 240 nm, slit width $\cong$20 cm^{-1}, number of pulses averaged 24 000. The second from the bottom spectrum derives from subtracting the CH_3CN Raman spectrum from the 10^{-6} M pyrene Raman spectrum. The bottom difference spectrum derives from subtracting a water Raman spectrum from the Raman spectrum of a 10^{-7} M aqueous pyrene solution.

lack of change in the pyrene Raman intensities between the 10^{-3} M and 10^{-4} M solutions occurs because of the strong absorption of the laser beam within the sample solution. 90° scattering is used for these Raman measurements. Thus, the collection optics transfer an image of the laser beam passing through the sample onto the slit of the monochromator. The 10^{-3} M and 10^{-4} M solutions have an absorbance at 240 nm of ca. 1000 cm^{-1} and 100 cm^{-1}, respectively. Thus, 90% of the Raman scattering occurs within a 10 μm and 100 μm height in the sample for the 10^{-3} M and 10^{-4} M solutions, respectively. Since the entire 100 μm illuminated sample height is imaged into the monochromator and the same numbers of pyrene molecules are sampled by the laser beam as it is attenuated through the sample, essentially identical Raman intensities for pyrene are observed. The increased volume of the CH_3CN solvent sampled accounts for the increased Raman intensity for CH_3CN. For the lower concentration solutions the effective illuminated sample volume height overfills the slit acceptance height, and a decrease in the detected pyrene Raman intensities occurs. Thus, the 10^{-5} M solution is dominated by

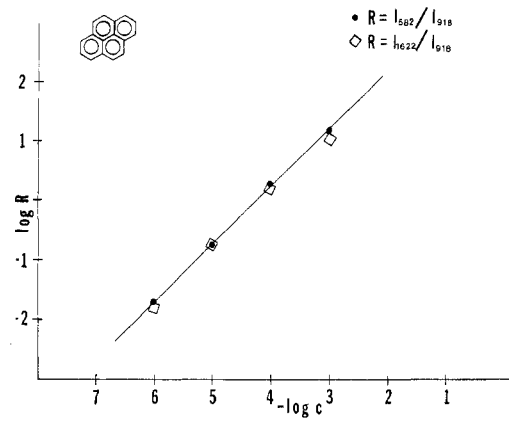

Figure 5. Concentration dependence of pyrene resonance Raman intensities. The circles indicate the ratio of intensity of 582-cm^{-1} pyrene peak to the 918-cm^{-1} intensity of the CH_3CN peak. The diamonds indicate the ratio of intensity of the 1622-cm^{-1} pyrene Raman peak to the intensity of the 918-cm^{-1} CH_3CN peak.

Raman scattering from CH_3CN and the intensities of the CH_3CN Raman peaks are essentially constant in the 10^{-4} to 10^{-6} M pyrene solutions.

The 10^{-6} M pyrene solution shows little evidence for pyrene Raman peaks. However, the difference spectrum between the 10^{-6} M pyrene solution and a pure CH_3CN solution, shown directly below that of the 10^{-6} M pyrene Raman spectrum, demonstrates that the most intense pyrene peaks at 1622 and 582 cm^{-1} are still visible even at 10^{-6} M concentration. The bottom spectrum in Figure 4 is of a 10^{-7} M pyrene solution in H_2O. This is a Raman difference spectrum in which a water Raman spectrum was subtracted from that of the 10^{-7} M aqueous pyrene solution. The 1622-cm^{-1} pyrene peak is evident in the 10^{-7} M solution as is the 1376-cm^{-1} peak which derives from CH_3CN, which was introduced during the preparation of the sample from the 10^{-4} M pyrene aliquot used to prepare the 10^{-7} M aqueous solution. As was observed in the 10^{-4} M solution Raman spectrum, the 1622-cm^{-1} pyrene and 1376-cm^{-1} CH_3CN Raman peaks show similar intensities. The sharp feature at ca. 1800 cm^{-1} derives from the incomplete subtraction of the water Raman peak.

Figure 5 shows the concentration dependence of pyrene resonance Raman intensity. The circles label the ratio of intensity of the pyrene 582-cm^{-1} peak to the 918-cm^{-1} acetonitrile peak, while the diamonds labels the ratio of intensity of the 1622-cm^{-1} pyrene peak to the 918-cm^{-1} acetonitrile peak. The curves are linear for both peaks with slopes of 1.0 and indicate the linear concentration dependence of pyrene resonance Raman intensities.

Significant selectivity for particular PAH's can be obtained by a judicious selection of excitation wavelength. Figure 6 shows the resonance Raman spectrum of pyrene excited at 240 nm at the maximum of its UV absorption band, and at 251 nm at a local minimum in the absorption spectrum. The ratio of sample absorbance at these two wavelengths is $A_{240}/A_{251} \cong 3.8$. The two Raman spectra shown have been approximately scaled such that the intensity of the acetonitrile peaks labeled "A" in the spectra are constant between the two excitation wavelengths. Changing the excitation wavelength from 240 nm to 251 nm results in the decrease in the intensity of the 582-cm^{-1} pyrene Raman peak by a factor of ca. 15, while the 1622-cm^{-1} peak has decreased by a factor of ca 7. These results indicate that by tuning the excitation wavelength within the absorption band of a mixture of PAH's, one can selectivity excite individual PAH's because of the strong excitation wavelength dependence of the resonance Raman intensities.

This resonance Raman intensity dependence, $I(\lambda)$ is related to the molecular electronic transition moment which is in turn

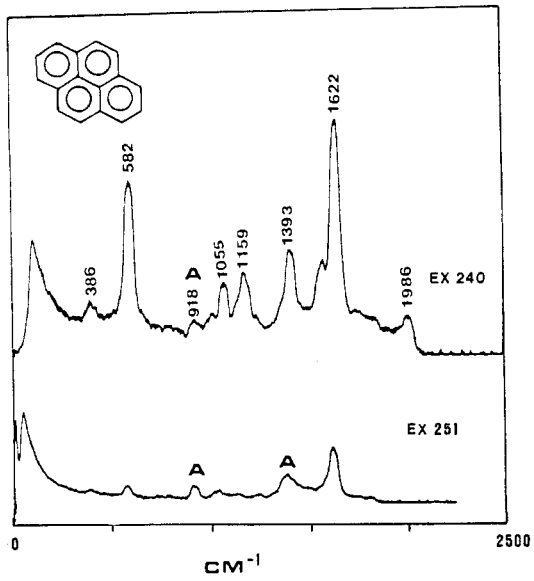

Figure 6. Excitation wavelength dependence of the resonance Raman spectra of pyrene. Top spectrum was obtained by exciting at the λ_{max} of the pyrene absorption spectrum: λ_{ex} 240 nm, average power 3.0 mW, slit width 11 cm^{-1}, number of pulses averaged 12 000. Bottom spectrum was obtained at a trough in the absorption spectrum: λ_{ex} 251 nm, average power 3.0 mW, slit width ≅11 cm^{-1}, number of pulses averaged 12 000.

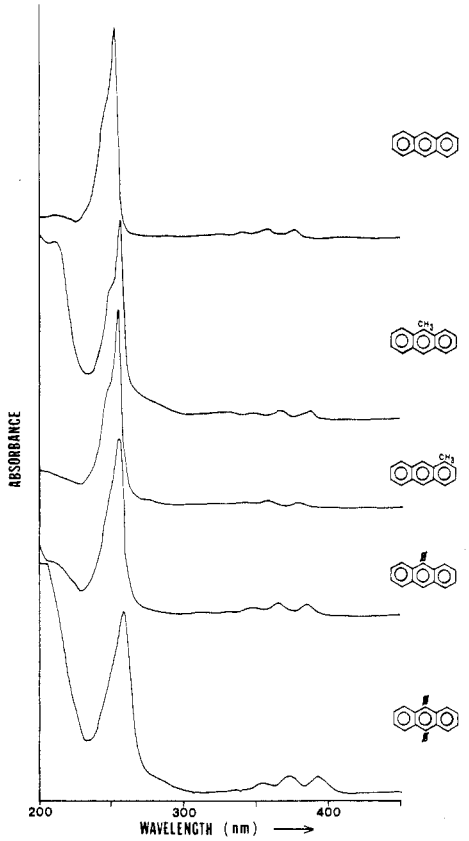

Figure 7. Absorption spectra of anthracene and its 2-methyl, 9-methyl, 9-phenyl, and 9,10-diphenyl derivatives.

related to the molar absorptivity, ϵ (*12, 13, 15*). In the simplest case $I(\lambda) \sim [\epsilon(\lambda)]^n$, where n has a value which depends upon the exact resonance Raman scattering mechanism. A consideration of ϵ at the two excitation wavelengths suggests that in the case of the 582-cm^{-1} peak, $n \sim 2$, while for the 1622-cm^{-1} peak $n \sim 1.5$. Thus, the selectivity available from the resonance Raman spectra is significantly greater than that for fluorescence where $n = 1$. We are in the process of quantifying the selectivity available for mixtures of PAH's by measuring

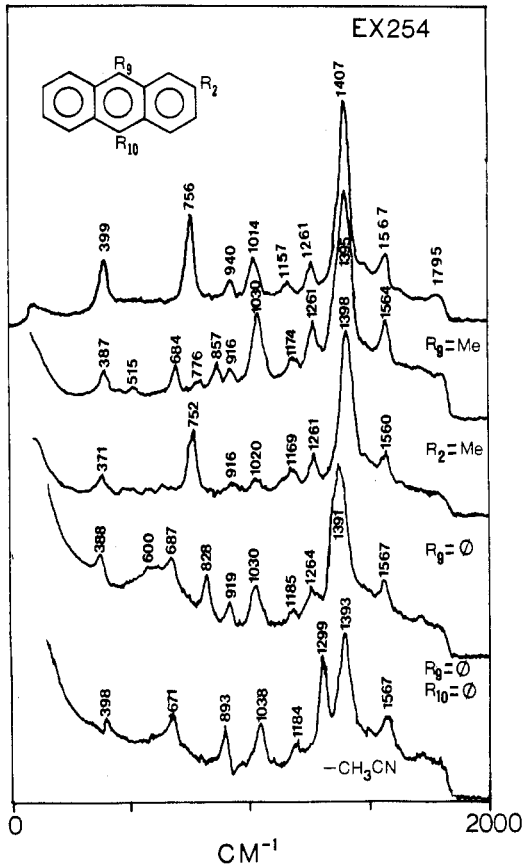

Figure 8. UV Resonance Raman spectra of anthracene and its 9-methyl, 2-methyl, 9-phenyl, and 9,10-diphenyl derivatives: λ_{ex} 254 nm, average power 3.0 mW, band-pass 11 cm^{-1}, number of pulses averaged 12 000, concentration ca. 10^{-3} M.

the resonance Raman excitation profiles for individual PAH species.

The resonance Raman spectra show a strong sensitivity to PAH structure and peripheral substitution. For example Figure 7 shows the absorption spectra of a series of anthracene derivatives, while Figure 8 shows the resonance Raman spectra of each of these derivatives excited at 254 nm, close to the λ_{max} of their strong absorption bands. The absorption spectra of these derivatives are very similar. The λ_{max} for anthracene occurs at 251 nm while those for 2-methyl-, 9-methyl-, 9-phenyl-, and 9,10-diphenylanthracene occur at 254, 254, 254, and 258 nm, respectively. It would be difficult to differentiate between these derivatives by using either absorption or fluorescence spectrometry.

The Raman spectra provide sufficient information, both from the vibrational frequencies and from the intensities, to differentiate between these derivatives. For example, the strongest lines in the Raman spectra occur at 1407 cm^{-1} for anthracene and at 1395, 1398, 1391, and 1393 cm^{-1} for the 9-methyl-, 2-methyl-, 9-phenyl-, and 9,10-diphenyl derivative, respectively. The 756-cm^{-1} peak in anthracene shifts to 752 cm^{-1} in 2-methylanthracene while it is absent in the other derivatives. A peak between 670 and 690 cm^{-1} is present for those derivatives with substitution at the nineth ring position while the feature at 760 cm^{-1} is absent. A unique feature in the 9,10-diphenyl derivative spectrum is the presence of a strong peak at 1299 cm^{-1}. Thus, from the resonance Raman spectrum excited at one wavelength, sufficient information is obtained to speciate between these very similar derivatives.

The vibrational modes observed in these spectra derive entirely from vibrations of the fused ring system; no enhancement is observed for C–H stretching in the 3000-cm^{-1} region, either from the fused ring peripheral hydrogens or from the phenyl ring hydrogens or from the methyl hydrogens. In

the phenyl-substituted derivatives no contribution is observed with excitation at 254 nm for phenyl ring vibrations. New peaks would be expected to occur near 1000 and 1600 cm^{-1}. This indicates that little conjugation occurs between the phenyl groups and the fused ring system to perturb the ground or the resonant excited state. This lack of conjugation between the phenyl groups and the anthracene moiety is consistent with the relatively small perturbation observed in the absorption spectrum of anthracene upon phenyl substitution. Resonance Raman excitation into other anthracene derivative absorption bands may result in the enhancement of internal vibrations of ring substituents. The differences in the relative intensities of the anthracene ring vibrations between these derivatives presumably result from differences in vibronic coupling and Franck-Condon factors due to differences in substitution on the fused ring. The frequency differences derive from perturbations in the vibrational normal modes.

The results shown in Figure 4 demonstrate that UV resonance Raman spectrometry can be used to detect and quantitate low concentrations of PAH's in solution. The 10^{-7} M pyrene sample corresponds to a pyrene concentration of 20 ppb. Within the illuminated sample volume, which is a cylinder ca. 0.4 mm high with a radius of ca. 0.1 mm, this corresponds to ca. 10^{-15} mol or 0.2 pg of pyrene. This concentration is not the detection limit since only 3 mW of laser power was used for these studies, and at these low concentrations a neglibible amount of the beam is attenuated by sample absorption. A significant increase in the Raman intensities would occur if the sample were contained in a multipass cell and the beam were reimaged into the scattering volume. This increase could be by a factor of 100. Further, because the laser excitation beam is defocused in the sample (radius ca 0.1 mm) only a small fraction of the beam width in the sample (<20%) is imaged through the entrance slit. Thus, the instrumentation could be significantly improved for these studies. The ultimate detection limit derives from interference from luminescence from the matrix, or for high laser intensities the detection limit will be determined by depletion of the ground state of the sample, or the appearance of nonlinear Raman or other phenomena (*14*). If the multipass cell were prepared such that the round trip transit time of the beam through the cell were long compared to the lifetime of the PAH excited state, the ultimate detection limit would derive directly from shot noise contributed by matrix luminescence.

In the case of the 10^{-7} M solution, the S/N ratio for the 1622-cm^{-1} pyrene peak is >15. This signal to noise ratio is obtained by assuming that the peak to peak noise is equal to 5σ, where σ is the standard deviation of the signal intensity. The peak intensity is about three times the line width of the spectral scan yielding $S/N \sim 15$. Ten additional passes of the beam through the cell and the use of five times the power (15 mW, within the normal specifications of our laser) should permit us to observe 10^{-9} M pyrene solutions (200 pptr) with an $S/N \sim 1$. The sensitivity demonstrated for pyrene is also observed for anthracene, the only other PAH whose concentration dependence we have measured.

CONCLUSIONS

The results presented indicate that UV resonance Raman spectrometry has potential for studies of PAH derivatives at trace parts-per-billion or parts-per-trillion concentrations. The Raman frequency and intensity information permits the structural differentiation of very similar species. One can selectively excite individual classes of PAH's in mixtures to separately quantitate individual species. This selectivity is superior to that available from conventional fluorescence techniques.

It should be possible to examine PAH species in complex matrices such as soot and in environmental water samples. Matrix fluorescence interferences are a potential problem and might limit the sensitivity of UV resonance Raman spectrometry for environmental samples. We are in the process of beginning an investigation into the viability of this application. One major advantage of resonance Raman spectrometry is that it is not subject to matrix effects such as quenching which plague fluorescence measurements; the lifetime associated with the Raman process is, in general, shorter than the collision times which are important in fluorescence quenching. It may be possible to speciate and quantitate PAH's in complex samples "as is" without extensive sample preparation.

ACKNOWLEDGMENT

We gratefully acknowledge Craig R. Johnson and Thanh Phung for technical help in these studies and Dianne Asher for help with the figures. We also thank David Hercules for samples of PAH's.

Registry No. Naphthalene, 91-20-3; phenanthrene, 85-01-8; pyrene, 129-00-0; anthracene, 120-12-7; 9-methylanthracene, 779-02-2; 2-methylanthracene, 613-12-7; 9-phenylanthracene, 602-55-1; 9,10-diphenylanthracene, 1499-10-1.

LITERATURE CITED

(1) Heidelberger, C. *Annu. Rev. Biochem.* **1975**, *44*, 79.
(2) Bjørseth, A., Ed. "Handbook of Polycyclic Aromatic Hydrocarbons"; Marcel Dekker: New York, 1983.
(3) Josefsson, B. In "Handbook of Polycyclic Aromatic Hydrocarbons"; Bjørseth, A., Ed.; Marcel Dekker: New York, 1983; pp 301–322.
(4) Wehry, E. L. In "Handbook of Polycyclic Aromatic Hydrocarbons"; Bjørseth, A., Ed.; Marcel Dekker: New York, 1983; pp 323–397.
(5) Long, D. A. "Raman Spectroscopy"; McGraw-Hill: New York, 1977.
(6) Clark, R. J. H.; Stewart, B. *Struct. Bonding (Berlin)* **1979**, *36*, 1.
(7) Carey, P. R. "Biochemical Applications of Raman and Resonance Raman Spectroscopies"; Academic Press: New York, 1982.
(8) Tu, A. "Raman Spectroscopy in Biology: Principles and Applications"; Wiley: New York, 1982.
(9) Asher, S. A. *Methods Enzymol.* **1981**, *76*, 371.
(10) Asher, S. A. *Appl. Spectrosc.*, in press.
(11) Asher, S. A.; Johnson, C. R.; Murtaugh, J. *Rev. Sci. Instrum.* **1983**, *54*, 1657.
(12) Albrecht, A. C. *J. Chem. Phys.* **1961**, *34*, 1476.
(13) Asher, S. A.; Johnson, C. R., submitted for publication in *J. Phys. Chem.*
(14) Levinson, M. J. "Introduction to Nonlinear Laser Spectroscopy"; Academic Press: New York, 1982.
(15) Tang, J.; Albrecht, A. C. In "Raman Spectroscopy: Theory and Practice"; Szymanski, H. A., Ed.; Plenum Press: New York, 1970; Vol. II, p 33.

RECEIVED for review September 30, 1983. Accepted January 3, 1984. We gratefully acknowledge support for this study from NSF Instrumentation Grant PCM-8115738 and NIH Grant 1R01 GM 30741-01. Acknowledgment is also made to the donors of the Petroleum Research Fund, administrated by the American Chemical Society. We also acknowledge starter grant support from a Cottrell Research Corp. Grant and BRSG Grant 2S07 RR 07084-16 awarded by the Biomedical Research Support Grant Program, Division of Research Resources, National Institutes of Health. We also acknowledge support from an American Cancer Society Instutional Grant provided to the University of Pittsburgh.